ADVANCED OPTICAL MATERIALS
www.advopticalmat.de

All-Dielectric Fiber Meta-Tip for Alignment-Tolerant Bidirectional Interconnect Between Single-Mode and Multi-Mode Fibers

*Jinke Li, Hongliang Li, Duk-Yong Choi, Jin Tae Kim, Woo-Bin Lee, and Sang-Shin Lee**

The growing demand for enhanced data transmission and network scalability requires connecting multi-mode fibers (MMFs) to single-mode fibers (SMFs). However, conventional fiber-optic connector systems face challenges such as one-way transmission, alignment issues, and bulkiness. In this study, an all-dielectric metasurface (MS)-based fiber-coupling system engineered to facilitate alignment-tolerant bidirectional optical interconnect at a communication wavelength of 1550 nm is proposed and demonstrated. The system features meticulously aligned fiber meta-tips incorporating an MS integrated onto SMF and MMF facets. The MS collimates the divergent beam emitted from the fiber facet and focuses the collimated beam propagating through free space, enabling bidirectional transmission of optical signals between the SMF and MMF. The achieved performance includes a coupling efficiency of −5.6 dB, optimal radial and axial tolerances of 40 and 600 µm, respectively, an extinction ratio of 13.8 dB, and a signal-to-noise ratio of 24.3 dB at 10.3 Gb s^{-1}. The proposed fiber meta-tips highlight the potential of lab-on-fiber technology for optical communication, trapping, and biological sensing.

1. Introduction

The significant demand for handling information in communication networks has challenged optical elements, particularly those with higher performance, broader bandwidths, and capacity for longer transmission distances.[1] Optical fibers play a major role in communication networks, serving as a transmission medium for short (inside buildings or data centers), and long (regional and intercontinental connections) distances in backbone networks.[2–5] Multimode fibers (MMFs) with a large core diameter are commonly used for short distances owing to their cost-effectiveness, easy light source coupling, and simplified alignment process.[6] However, MMFs exhibit modal dispersion and higher attenuation than single-mode fibers (SMFs).[7] Hence, to overcome the limitations of MMFs over long distances, SMFs are preferred owing to their lower attenuation and lack of modal dispersion. However, SMFs with smaller core sizes require the precise alignment of light sources, thus resulting in increased system complexity, and cost.[8] Both SMFs and MMFs offer unique advantages and have applications in global networks. The effective coupling of light between MMF and SMF poses a challenge owing to their differing mode-field diameters. Therefore, a device capable of achieving efficient coupling between the two fibers is essential for ensuring stability and reliability of optical telecommunications.

Fiber-optic connectors play a pivotal role in facilitating optical coupling owing to their effective installation and detachment, high durability, and enhanced robustness.[9,10] For physical contact fiber-optic connectors primarily employing butt-coupled SMFs with relatively small mode field diameters, potential issues include one-way transmission from small to large mode fields, susceptibility to damage, contamination of fiber facets, and misalignment between fibers.[11] As a compelling alternative, expanded beam technology has gained significant attention because of its distinct advantages including increased resistance to contamination and damage, along with enhanced structural tolerance.[11–13] Conventional fiber-optic beam expansion connectors heavily rely on the precise alignment of optical fibers with optical lenses, which are crucial for generating, and transmitting an amplified collimated beam, and enabling bidirectional transmission. However, such connectors suffer from several drawbacks including limited integration, high sensitivity to alignment by environmental instability, and bulky size.[14–18]

J. Li, H. Li, W.-B. Lee, S.-S. Lee
Department of Electronic Engineering
Kwangwoon University
Seoul 01897, Republic of Korea
E-mail: slee@kw.ac.kr

J. Li, H. Li, W.-B. Lee, S.-S. Lee
Nano Device Application Center
Kwangwoon University
Seoul 01897, Republic of Korea

D.-Y. Choi
Department of Quantum Science and Technology
Research School of Physics
Australian National University
Canberra, ACT 2601, Australia

J. T. Kim
Quantum Technology Research Department
Electronics and Telecommunications Research Institute
Daejeon 34129, Republic of Korea

The ORCID identification number(s) for the author(s) of this article can be found under https://doi.org/10.1002/adom.202401712

DOI: 10.1002/adom.202401712

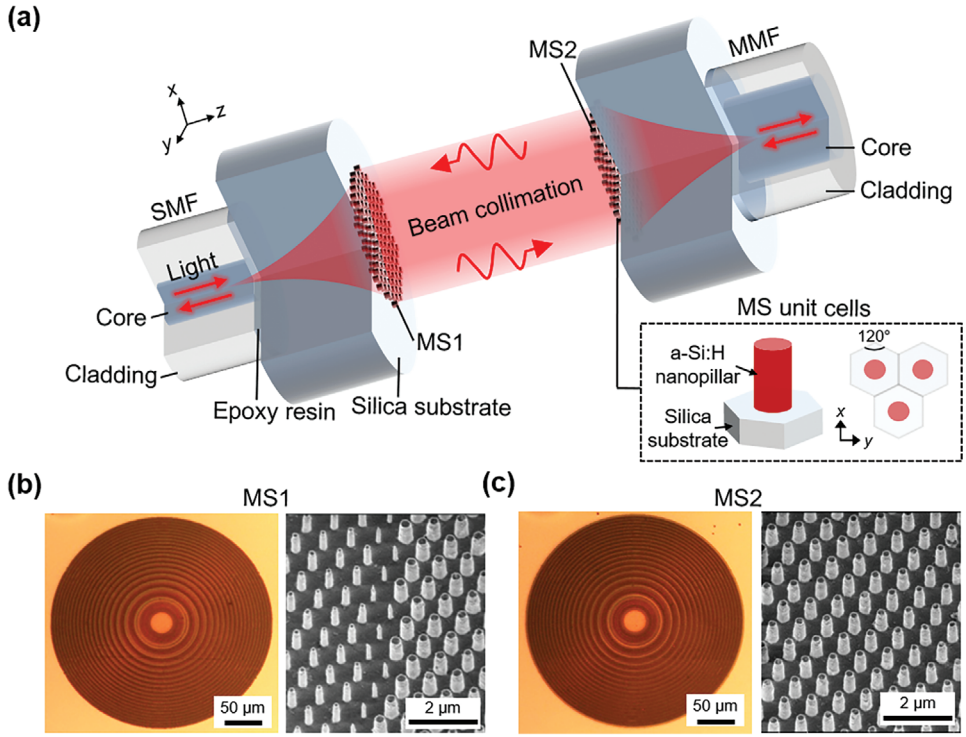

Figure 1. a) Schematic of the proposed all-dielectric MS-based fiber coupling system comprising two MSs, denoted as MS1 and MS2, integrated with an SMF and MMF, respectively; Microscope and scanning electron microscope images of the fabricated b) MS1 and c) MS2.

A metasurface (MS), an ultrathin optical component comprising an array of artificial meta-atoms, significantly enhances the interaction between photons and matter by meticulously designing the geometric structure, arrangement, and materials of meta-atoms.[19] A diverse range of MS-based devices, including beam deflectors,[20] polarizers,[21] modulators,[22] and meta-holograms,[23] have been developed, capitalizing on precise beam manipulation offered by MS over the fundamental properties of light. Recently, by leveraging the MS-integrated fiber concept, various devices such as fiber-tip lenses,[24–26] surface plasmon resonance sensors,[27,28] optical tweezers,[29] polarimeters,[30] and polarization converters[31] have been developed, highlighting the advantages of easy integration, enhanced light manipulation, and compact size. Notably, MS-integrated fibers have demonstrated efficacy in optical data signal mediation.[32] Hence, embracing an MS-on-a-fiber configuration presents a promising solution to meet the requirements of compact and bidirectional optical coupling and telecommunication between SMFs and MMFs.

In this work, we propose and realize an all-dielectric MS-based fiber-coupling system designed for alignment-tolerant bidirectional optical interconnect at a communication wavelength of 1550 nm. The apparatus features two precisely aligned fiber meta-tips, each of which integrates a carefully designed MS within SMF and MMF facets. The MS collimates the divergent beam emitted from the fiber facet and focuses the collimated beam propagating through free space, thereby serving as a bidirectional medium for transmitting optical signals between the SMF and MMF. The efficacy of the fiber coupling scheme is experimentally evaluated by assessing alignment tolerance and optical interconnection performance. Our findings illuminate a compact and efficient solution for fiber coupling, underscoring its potential to revolutionize optical communication networks and advance high-speed data transmission and photonics applications.

2. Proposed MS-Based Fiber Coupling System and its Design

As depicted in **Figure 1a**, the proposed all-dielectric MS-based fiber coupling system comprised two MSs, denoted as MS1 and MS2, which are integrated with SMFs (Corning SMF-28e) and MMFs (GIF625, Thorlabs), respectively. MS1 and MS2 were affixed to the silica substrates of the fibers using epoxy resin (NOA 61, Thorlabs). Initially, the light was launched from the SMF facet into the epoxy and glass substrates, causing it to disperse. Subsequently, MS1 intercepted the divergent light and collimated it with the surrounding air. Further, MS2 gathered the collimated light and precisely directed it to the MMF core, concluding the optical coupling process from SMF to MMF and mirroring the process from MMF to SMF. MS1 and MS2 comprising SMF and MMF meta-tips were designed based on hydrogenated amorphous silicon (a-Si:H) nanopillars owing to their low cost, high refractive index (RI), and compatibility with complementary metal-oxide-semiconductor processes.[33] MS1 and MS2 were fabricated using electron beam lithography (EBL), as detailed in the Experimental section, and are shown in Figure 1b,c, respectively. The desired phase profile of MS1 was expressed as $\varphi_{MS1}(x, y) = -[\frac{2\pi n}{\lambda}(z + \frac{x^2+y^2}{2R(z)}) - tan^{-1}(\frac{z}{z_0})]$, where (x, y) represents the coordinates corresponding to the center of each unit cell in the middle

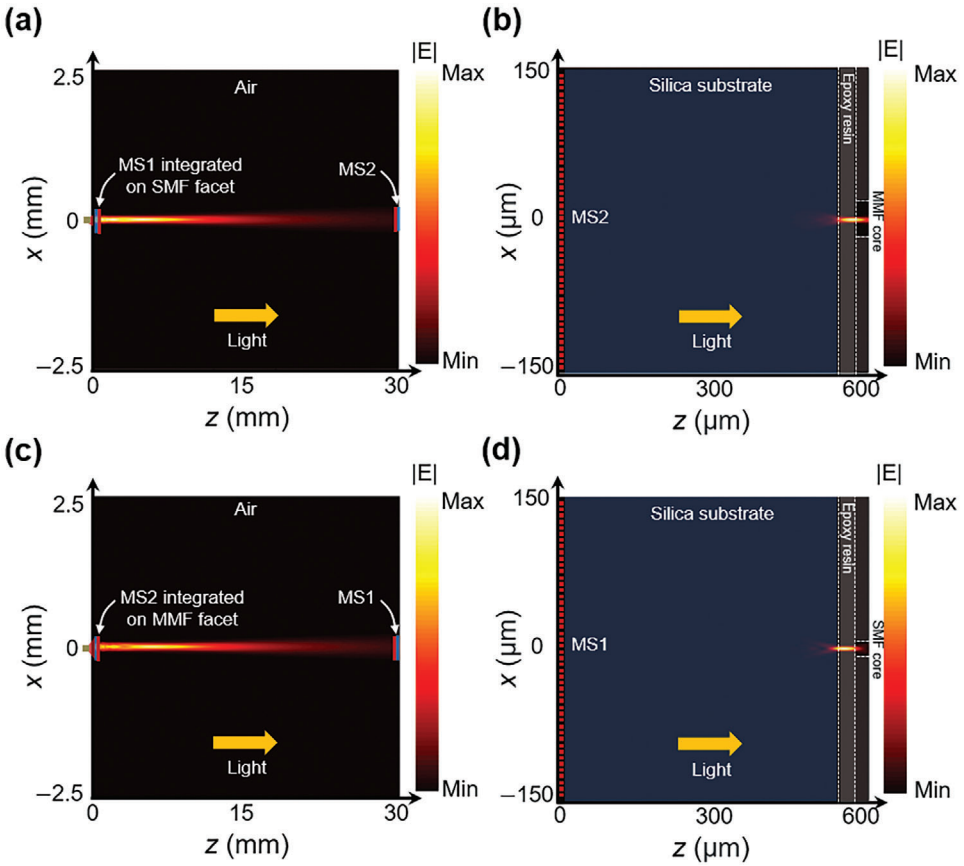

Figure 2. Simulation results for the developed fiber meta-tip: Electric field distributions in the *xz*-plane after a) beam collimation by MS1, and b) beam focusing by MS2 ($y = 0$); Electric field distributions in the *xz*-plane after c) beam collimation by MS2 and d) beam focusing by MS1 ($y = 0$).

of MS1, $R(z)$ is the radius of curvature at an axial distance of z, z_0 is the Rayleigh length, and n is the RI of the dielectric spacer between MSs and fiber facets. The desired phase profile of MS2 was expressed as $\varphi_{MS2}(x, y) = [\frac{2\pi n}{\lambda}(f - \sqrt{f^2 + x^2 + y^2})]$, where (x, y) represents the coordinates corresponding to the center of each unit cell in the middle of MS2 and f is the focal length of MS2. The fundamental mode of SMF was approximated using a Gaussian beam at the output fiber facet.[34] The inverted phase profile of the Gaussian beam after propagation through the epoxy resin and silica substrate was used as the target phase profile for MS1 to enable beam collimation.[35] The collimated beam from MS1 was focused onto the MMF core when the fixed distance between the MMF facet and MS2 corresponded to f.[32] Due to optical path reversibility, the process theoretically achieved reverse coupling from the MMF to the SMF.

Numerical 3D simulations were conducted to validate the functionality of the proposed fiber meta-tips using commercial finite-difference time-domain software, FDTD Solutions (Ansys Lumerical, Canada). For simulation, the core and cladding of the SMFs were set to 8.2 and 125 μm in diameter, respectively, with corresponding RIs of 1.4504 and 1.4447 at a wavelength (λ) of 1550 nm. For the MMFs, the core and cladding diameters were 62.5 and 125 μm, respectively. The RI at the core center was 1.4667, while that of the outer cladding was 1.4447 at $\lambda = 1550$ nm. The diameters of the fiber core and cladding were selected in accordance with simulations and experimental validation (Table S1 and Figure S2, Supporting Information). The thicknesses of the silica substrate and epoxy resin were 530 and 30 μm, respectively. The values were carefully selected to ensure beam divergence compensation during propagation from the fiber facet to the MS.[36] The RIs of the silica substrate and epoxy resin were 1.44 and 1.56 at $\lambda = 1550$ nm, respectively. Both MS1 and MS2 were designed for a diameter of 300 μm to ensure their ability to effectively accommodate light emerging from the fibers. Through multiple careful simulations that take account into the far-field angle of the transmitted light and the focal length of the received light in the gap between the MS and fiber facet, $R(z)$ for MS1, and f for MS2 were finally set to 562 and 560 μm, respectively (Tables S2, S3, and Figure S2, Supporting Information). The impact of the epoxy resin layer on the Gaussian beam emitted from the fiber facet was considered (discussed in Experimental Section). **Figure 2**a,b illustrate the calculated electric field distributions in the *xz*-plane for the optical coupling process from SMF to MMF. The full-width-at-half-maximum (FWHM) beam divergence angle is a key metric for evaluating collimation quality. A smaller FWHM angle indicates reduced divergence and better collimation, whereas a larger FWHM angle reflects greater divergence and poorer collimation.[37] Initially, MS1 collimated the

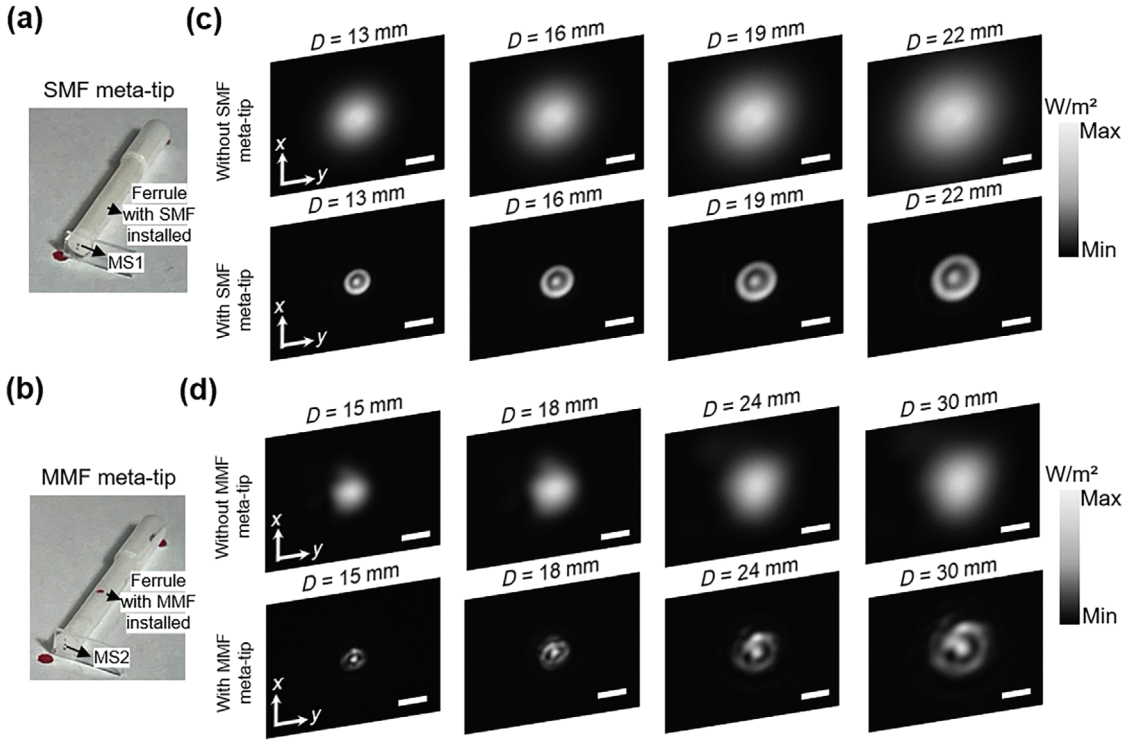

Figure 3. Photographs of the completed a) SMF meta-tip and b) MMF meta-tip samples; Intensity distributions observed for varying *D* between the NIR camera and the c) SMF meta-tips, spanning from 13 to 22 mm; Intensity distributions examined for different *D* between the NIR camera and d) the MMF meta-tips, ranging from 15 to 30 mm (Scale bar: 1 mm).

divergent Gaussian beam emitted from the SMF facet, reducing the FWHM angle from 11.25° to 1.20°. Subsequently, MS2 received the collimated beam 30 mm along the *z*-direction from MS1 and focused it onto the MMF core at a focal distance of 558 µm, considering the influence of light propagation through the interface between the silica substrate and epoxy resin. Similarly, Figure 2c,d illustrates the calculated electric field distributions in the *xz*-plane for the optical coupling process from the MMF to the SMF. Herein, MS2 performed the initial collimation of the divergent Gaussian beam emitted from the MMF facet, thereby significantly reducing the FWHM angle from 5.96° to 0.92°. Subsequently, MS1 received the collimated beam 30 mm along the *z*-direction from MS2 and focused it into the SMF core at a focal distance of 554 µm. The simulation results indicated the establishment of unobstructed optical pathways by the MS between the SMF and MMF, thus facilitating bidirectional light coupling and validating the theoretical viability of the coupling scheme.

3. Experimental Results and Discussion

The completed assembly of the SMF and MMF fiber meta-tips, illustrated in **Figure** 3a,b, involved affixing the MS1 and MS2 components to the SMF and MMF using ultraviolet-curable epoxy within ferrules to enhance contact areas, as discussed in Experimental Section. The apparatus employed to characterize both the fabricated MSs is detailed in Experimental Section as well. A sequence of images representing the intensity distributions in the *xy*-plane was captured by translating the near-infrared (NIR) camera (ABA-001IR, AVAL GLOBAL) along the optical axis (*z*-axis). Figure 3c presents the intensity distributions at distances (*D*) from 13 to 22 mm between the NIR camera and the SMF meta-tip. Similarly, Figure 3d shows the intensity distributions for distances ranging from 15 to 30 mm between the NIR camera and the MMF meta-tip. The results illustrated that MS1, comprising the SMF meta-tip, collimated the divergent Gaussian beam emitted from the SMF facet, thereby reducing the FWHM angle from 11.25° to 3.76°. Similarly, MS2 comprising the MMF meta-tip collimated the divergent multi-mode beam emitted from the MMF facet, decreasing the FWHM angle from 5.96° to 2.40°. Without SMF meta-tip collimation, the beam diameter increased from 2.14 to 3.91 mm as *D* increased from 13 to 22 mm; under collimation, it ranged from 0.83 to 1.41 mm. Similarly, without MMF meta-tip collimation, the beam diameter increased from 1.09 to 2.67 mm as *D* increased from 15 to 30 mm, and under collimation, the beam diameter changed from 0.61 to 1.48 mm. These findings demonstrate that a smaller FWHM angle results in a strengthened power distribution leading to a diminished mode field, thus enhancing the coupling efficiency of the receiver. The presence of a ring surrounding the collimated beam could have resulted in undesired diffraction during light collimation due to the optical axis and focal length deviation of the fiber core and MS.[38] The dispersion characteristics of the fabricated MS were evaluated (Figure S3, Supporting Information), revealing that the device exhibited no significant dispersion across the C and L bands, consistent with the expected dispersion-free performance. The polarization characteristics of the fabricated MS were also evaluated (Figure S4, Supporting Information),

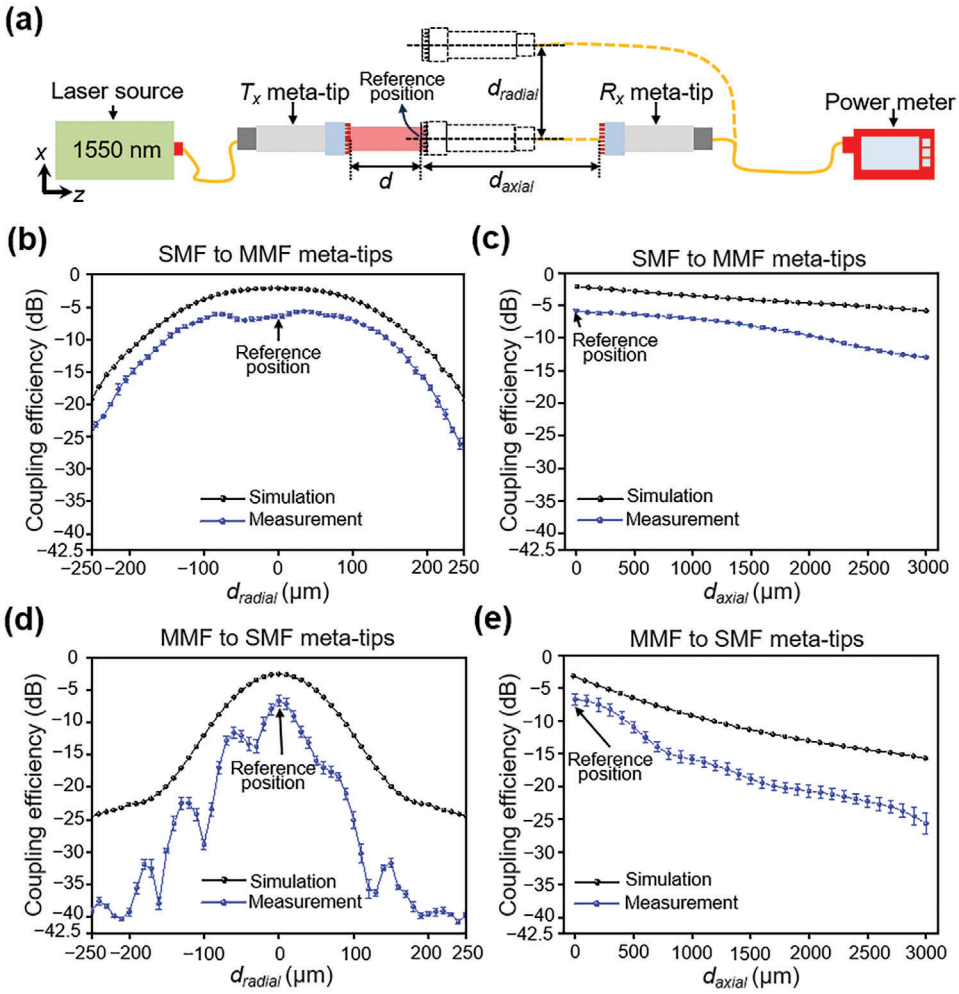

Figure 4. a) Experimental setup for testing the coupling efficiency between proposed SMF and MMF meta-tips; Impact of b) radial, and c) axial mismatch on the coupling efficiency for SMF to MMF meta-tips; Impact of d) radial and e) axial mismatch on the coupling efficiency for MMF to SMF meta-tips.

confirming that the device exhibited excellent polarization insensitivity as intended.

To evaluate its stability and reliability, the proposed MS-based fiber coupling system was assessed under three distinct input light power conditions emitted from the fiber facet using a custom-designed setup, as illustrated in **Figure** 4a. The alignment tolerance of the system was assessed in terms of the coupling efficiency. Figure 4b,c depicts the impact of radial and axial mismatch on the coupling efficiency, respectively, and demonstrate a decreasing efficiency with increasing discrepancies. Reverse transmission functionality was verified by analyzing the impact of radial and axial mismatches on the coupling efficiency for the MMF-to-SMF meta-tips, as shown in Figure 4d,e. The fluctuation in the mismatch curve was attributed to the excitation of multiple modes of light in MMF, causing an uneven energy distribution in the overall beam profile. The transmission performance of the proposed fiber coupling system across different fiber meta-tips was further evaluated by assessing the radial and axial mismatches for both MMF to MMF meta-tips and SMF to SMF meta-tips (Figure S5, Supporting Information).

The observed performance for the combination of transmitter (T_x) and receiver (R_x) is listed in **Table** 1. The obtained data indicated that the proposed system achieved an optimal coupling efficiency of −5.65 dB. The observed loss was attributed to factors such as signal attenuation due to multimode destructive interference in the MMF, material absorption, discrepancies in the focused beam position caused by fabrication errors, and Fresnel losses at various interfaces, including those between the fiber, epoxy, silica substrate, and air. When tolerance was reasonably assessed with reference to an excess insertion loss of 0.5 dB,[18] the optimal radial and axial tolerances were 40 and 600 μm, respectively, particularly when using MMF at the receiving section. The structural tolerance was relatively relaxed both transversely and longitudinally. The proposed device was compared with conventional physical contact fiber-optic connectors and extended bundle connectors in terms of compatibility, flexibility, directionality, and dimensions as outlined in **Table** 2. Although the physical contact connectors are compact and suitable for integration,[39,41] they support only one-way transmission, which limits their flexibility. Extended bundle connectors facilitate bidirectional transmission by matching the mode field diameter of the expanded

Table 1. Performance of the proposed MS-based fiber coupling system.

T_x [x: MS1-SMF meta-tip or MS2-MMF meta-tip]	R_x	Coupling efficiency [Db]	Distance between T_x and R_x meta-tip: d [mm]	Tolerance of d_{radial} [μm] [excess insertion loss ≤0.5 dB]	Tolerance of d_{axial} [μm] [excess insertion loss ≤0.5 dB]
MS1-SMF meta-tip	MS2-MMF meta-tip	−5.6	8.0	25	450
MS2-MMF meta-tip	MS1-SMF meta-tip	−6.7	7.8	12	150
MS2-MMF meta-tip	MS2-MMF meta-tip	−6.0	8.1	40	600
MS1-SMF meta-tip	MS1-SMF meta-tip	−7.9	7.5	10	110

beam.[18,42–44] However, traditional lens-based expansion methods suffer from disadvantages in terms of size and integration. Meanwhile, the proposed fiber meta-tip offers notable advantages in size, rendering it more suitable for integration into miniaturized photonic devices. The return loss of the assembled fiber meta-tip was measured using a fiber optic circulator (6015-3-FC, Thorlabs) and was given by $10\log_{10}(\frac{P_{ref}}{P_{inc}})$, where P_{ref} is the reflected optical power and P_{inc} is the incident optical power.[45] The return loss for the SMF and MMF meta-tip was measured as −65.3 and −80.2 dB, respectively, signifying that the transmission performance of the assembled device is superior. The coupling efficiency over a time period of 2 h and the impact of disconnect-reconnect cycles of 20 times on the working efficiency was monitored, as shown in Figure S6 (Supporting Information). The variations in coupling efficiency were 0.7 dB for SMF-to-MMF and 0.5 dB for MMF-to-SMF meta-tips, confirming their satisfactory system stability and reliability. The variations in the working efficiency over the disassembly cycles were 2.4% and 5.0% for the SMF and MMF meta-tips, respectively, underpinning excellent connection stability, mechanical reliability, and long-term durability.

To investigate the performance of optical interconnects that utilize the proposed fiber meta-tips, a pair of fiber meta-tips comprising precisely aligned SMF and MMF meta-tips positioned 8 mm apart was integrated to establish a free-space optical interconnect. A laser emitting light at $\lambda = 1550$ nm was modulated using an electro-optic modulator (MX-LN-10, iXblue), with the electrical signal supplied by a pulse pattern generator (BA-4000, EXFO) and amplified by a digital radio frequency amplifier (DR-DG-10-MO, iXblue). The prepared coupling system was tested to transmit a 2^{31}-1 pseudorandom bit sequence signal, and optical eye patterns were analyzed by monitoring the transmitted optical signals using a digital communication analyzer (DAC-J 86100C, Agilent). **Figure 5a** depicts the observed eye patterns for SMF to MMF meta-tips at data rates of 10.3 and 12.5 Gb s^{-1}, with corresponding measured extinction ratios of 13.5 and 13.6 dB, and signal-to-noise ratios of 23.3 and 21.6 dB, respectively, thereby indicating reliable data transmission. To verify the reversibility of data transmission, the eye patterns for MMF to SMF meta-tips were examined, at data rates of 10.3 and 12.5 Gb s^{-1}, as depicted in Figure 5b. The extinction ratios were 13.8 and 13.6 dB, with signal-to-noise ratios of 24.3 and 21.6 dB, respectively. The established coupling scheme demonstrated the potential to achieve a maximum extinction ratio of 13.8 dB and signal-to-noise ratio of 24.3 dB at a data rate of 10.3 Gb s^{-1}, which highlights its capability for high-speed and reliable data transmission.

4. Conclusion

In summary, we demonstrate a pioneering all-dielectric MS-based fiber coupling system featuring two precisely aligned fiber meta-tips crafted from an integrated MS within the fiber facet which successfully facilitates alignment-tolerant bidirectional optical interconnect at a telecommunication wavelength of 1550 nm. The telecommunication performance of the coupling scheme relies on beam collimation and focusing controlled by MS, which was validated experimentally by evaluating alignment tolerance and optical interconnectivity. The device achieved a coupling efficiency of −5.6 dB, optimal radial and axial tolerances of

Table 2. Comparison of the proposed device with other physical contact fiber-optic connectors and extended bundle connectors.

Type	Connection method	Compatibility	Flexibility	Directionality	Volume
Physical contact fiber-optic connectors	Fusion splice coupler[39]	SMF to MCF[a)]	Non-detachable	Unidirectional	$\approx(\pi \times 0.0625^2 \times 4 \approx 0.0491)$ mm^3
	Fiber adapter coupler[40]	MCSMF to MMF[b)]	Detachable	Unidirectional	$\approx(10 \times 10 \times 6 \approx 600)$ mm^3
	Plug-and-play coupler[41]	SMF to waveguide	Detachable	Unidirectional	$\approx(0.16 \times 0.023^2 \approx 8.46 \times 10^{-5})$ mm^3
Extended bundle connectors	Gapless fiber-lens interface[18]	SMF to SMF	Detachable	Bidirectional	$\approx(4/3 \times \pi \times 1.5^3 \approx 14.1)$ mm^3
	Graded-index lens interface[42]	SMF to the saturable absorber	Detachable	Bidirectional	$\approx(0.9^2 \times \pi \times 4.5 \approx 11.5)$ mm^3
	Double-combined collimating lenses[43]	TECF to TECF[c)]	Detachable	Bidirectional	$\approx(1^2 \times \pi \times 5 \approx 15.7)$ cm^3
	Double-combined collimating lenses[44]	LCMF to LCMF[d)]	Detachable	Bidirectional	$\approx(25^2 \times \pi \times 5 \times 2 \approx 1.96 \times 10^4)$ mm^3
	Double-combined collimating MS (this work)	SMF to MMF	Detachable	Bidirectional	$\approx(0.5 \times 2.5 \times 2.5 \approx 3.1)$ mm^3

[a)] multi-core fiber; [b)] modal conditioning single-mode fiber; [c)] thermally-diffused expanded core fiber; [d)] large core multimode fiber.

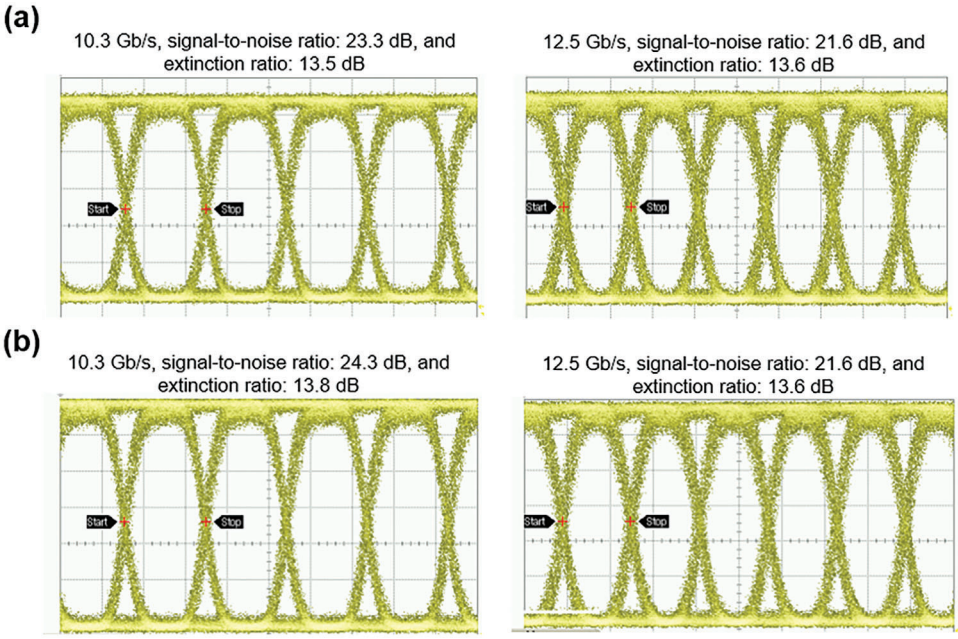

Figure 5. Observed eye patterns for high-speed data transmission a) from SMF to MMF meta-tips and b) from MMF to SMF meta-tips.

40 and 600 μm, with a peak extinction ratio and signal-to-noise ratio of 13.8 and 24.3 dB, respectively, at 10.3 Gb s^{-1}, thus confirming its high-speed and reliable data transmission. The proposed scheme of an all-dielectric MS integrated with fibers presents a promising connection between fiber-optic methodologies and the burgeoning realms of flat optics and photonics, thus laying the groundwork for the advancement of highly integrated compact photonic devices/systems. As a proof of concept, our next goal is to integrate the proposed MS coupling structure into practical fiber-optic connection systems and evaluate its stability under various environmental conditions in terms of temperature, humidity, and pressure.

5. Experimental Section

Fabrication of the Proposed MS1 and MS2: The proposed MS1 and MS2 comprising SMF and MMF meta-tip structures were fabricated through a meticulous process on a 530-μm-thick silica substrate, which served as a precisely controlled dielectric spacer (Figure S7, Supporting Information). Before fabrication, the substrate was thoroughly cleaned using a combination of acetone, isopropyl alcohol, and deionized water to enhance its adhesion to the a-Si:H film. Subsequently, a 920-nm-thick layer of a-Si:H was meticulously deposited onto the substrate using plasma-enhanced chemical vapor deposition (Plasmalab 100, Oxford). To define the desired features, a positive-electron-beam resist (ZEP520A, Zeon Chemicals) was carefully spin-coated onto the substrate. Additionally, an Espacer coating (300Z, Showa Denko) was applied to prevent charging during electron beam exposure. Using EBL with a Raith150 system, either the MS1 or MS2 alignment mark was intricately patterned onto the resist, followed by development in ZED-N50. To create an essential mask for subsequent processing, a 60-nm-thick Al film was meticulously deposited onto the substrate via electron beam evaporation (Temescal BJD-2000) and precisely patterned by removing the resist using a solvent (ZDMAC from Zeon Co.). The patterned Al layer served as a robust mask during dry etching to enable the transfer of the designed pattern onto the underlying a-Si:H layer. The dry etching process was performed using a fluorine-based inductively coupled plasma reactive ion etching system (Oxford Plasmalab System 100), with etching conditions meticulously optimized by precisely controlling a mixture of CHF_3 and SF_6 gases. Thus, nanopillars with high aspect ratios and vertical sidewalls were formed. Subsequently, a wet etching step was performed to eliminate residual Al from the patterned nanopillars, thereby finalizing the fabrication process for either MS1 or MS2.

Impact of the Epoxy Resin Layer on the Gaussian Beam Emitted from the Fiber Facet: Figure S8a–c (Supporting Information) depicts the calculated electric field distributions in the *xz*-plane. The distributions corresponded to the light emitted from the facet of an SMF as it traversed the epoxy and glass substrates on its way to the surrounding air. Notably, when the divergent Gaussian beam emitted from the SMF facet entered the glass substrate from the epoxy, its FWHM angle increased from 10.40° to 11.25°. Subsequently, as light transitioned from the silica substrate to air, its FWHM angle further expanded from 11.25° to 12.10°. Figure S8d–f shows the calculated electric field distributions in the *xz*-plane. The distributions corresponded to the light emitted from the MMF facet as it traversed the epoxy and silica substrates on its way to the surrounding air. Notably, as the divergent Gaussian beam (considering fundamental TE mode) emitted from the MMF facet entered the silica substrate from the epoxy, its FWHM angle increased from 4.92° to 5.96°. Furthermore, upon transitioning from the silica substrate to air, the FWHM angle experienced an additional expansion, rising from 5.96° to 6.56°.

Assembly of the Fiber Meta-Tip: Flat MS1 and MS2 were precisely aligned and attached to the SMF and MMF, respectively. Further, they were embedded in a ferrule (TTI Fiber Communication Tech. Co., Ltd.) with the assistance of a vision system. MS was securely held in place using a holder, while the ferrule (length and outer diameter of 22 and 2.0 mm, respectively) was secured using a vacuum mount on top of a motorized translation stage. Finally, the MS substrate with a footprint of ≈14 mm^2 was bonded to the fiber ferrule using ultraviolet-curable epoxy to complete the assembly of the fiber meta-tips. As shown in Figure S9a, the gap between the MS and the fiber facet inside of the ferrule comprises a 35-μm-thick epoxy layer in conjunction with a 530-μm-thick silica substrate. Figure S9b,c presents the calculated changes in the FWHM angle (θ) of the light propagating through the silica substrate, and the beam diameter (w) of the light reaching the MS with the epoxy thickness (d_{epoxy_resin}). The results reveal that d_{epoxy_resin} has a minimal effect on θ, while having a relatively

larger impact on *w*. To control the gap length, a vision system has been employed to monitor the bonding of the epoxy resin between the MS substrate and the fiber-installed ferrule. Initially, a uniform layer of epoxy was applied to the ferrule. The silica substrate was then positioned over the ferrule, ensuring complete coverage of the epoxy-coated area. Precise alignment was achieved by vertically aligning the center of the fiber core within the ferrule with the center of the MS atop the silica substrate. When alignment was secured, the silica substrate is gently pressed against the ferrule to regulate the epoxy thickness to the predetermined value of ≈30 µm. The epoxy was then cured by ultraviolet light, completing the fiber meta-tip assembly. It was noted the MS was designed with a diameter of 300 µm to safely accommodate the incident light beam.

Experimental Characterization of the Fabricated MSs: A distributed feedback laser (ALCATEL, A1905LMI) equipped with a collimator (Fiberpia, FC/PC) was used as the light source. The incident light was focused onto the MSs using an objective lens (Thorlabs, AC254-050-C-ML) with a diameter of ≈300 µm. An optical power meter (Thorlabs PM200) was used to monitor the efficacy of the proposed MSs. For MS1, three samples were evaluated, yielding focusing efficiencies of 51.1%, 58.4%, and 60.6%, with an average efficiency of 56.7%. Similarly, three samples were assessed for MS2, revealing focusing efficiencies of 57.1%, 60.0%, and 58.3%, with an average efficiency of 58.5%.

Supporting Information

Supporting Information is available from the Wiley Online Library or from the author.

Acknowledgements

This work was supported by the Basic Science Research Program through the National Research Foundation of Korea (NRF) funded by the Ministry of Education (No. 2018R1A6A1A03025242) and Ministry of Science and ICT (RS202400334779), a research grant of Kwangwoon University in 2024, and an Electronics and Telecommunications Research Institute (ETRI) grant (24YS1210, Development of Fundamental Technology for a Photonic Quantum Computing System to Solve #P-Complete Problem). Fabrication was performed at the ACT node of the Australian National Fabrication Facility.

Conflict of Interest

The authors declare no conflict of interest.

Data Availability Statement

The data that support the findings of this study are available from the corresponding author upon reasonable request.

Keywords

alignment-tolerant, bidirectional, compact, extended bundle connector, fiber meta-tip, multi-mode fibers, single-mode fibers

Received: June 28, 2024
Revised: September 20, 2024
Published online:

[1] D. Garg, A. Nain, *J. Opt. Commun.* **2023**, *44*, s1535.
[2] F. Idachaba, U. Dike, O. H. Ike, *Proc. World Congr. Eng.* **2014**, *1*, 978.
[3] M. Arumugam, *Pramana. J. Phys* **2001**, *57*, 849.
[4] P. Sharma, M. Singh, *Int. J. Emerg. Technol. Adv. Eng.* **2013**, *3*, 113.
[5] M. Ding, D. Fan, W. Wang, Y. Luo, G. D. Peng, *Handbook of Optical Fibers*, Springer, Singapore **2018**, *1*, 1099.
[6] R. E. Freund, C. A. Bunge, N. N. Ledentsov, D. Molin, C. Caspar, *J. Lightwave Technol.* **2010**, *28*, 569.
[7] M. B. Shemirani, J. M. Kahn, *J. Lightwave Technol.* **2009**, *27*, 5461.
[8] P. Sharma, S. Pardeshi, R. K. Arora, M. Singh, *Int. J. Emerg. Technol. Adv. Eng.* **2013**, *3*, 113.
[9] M. Childers, M. Hughes, T. Satake, *Proc. SPIE* **2014**, *8991*, 125.
[10] M. Karppinen, A. Tanskanen, J. Ollila, V. Heikkinen, presented at Proc. IEEE Avionics Fiber Optics and Photonics Technology Conf., FL, USA, September **2012**.
[11] A. A. Kazemi, *Proc. SPIE* **2014**, *9202*, 92021.
[12] J. Niu, J. Xu, *Opt. Commun.* **2007**, *274*, 315.
[13] P. Chanclou, H. Ramanitra, P. Gravey, M. Thual, *J. Lightwave Technol.* **2002**, *20*, 836.
[14] S. C. Shen, C. T. Pan, K. H. Liu, C. H. Chao, J. C. Huang, *J. Micromech. Microeng.* **2009**, *19*, 125017.
[15] W. Yu, X. C. Yuan, *IEEE Photon. Technol. Lett.* **2003**, *10*, 1410.
[16] S. H. Ghasemi, M. R. Hantehzadeh, J. Sabbaghzadeh, D. Dorranian, V. Vatani, A. Babazadeh, K. Hejaz, A. Hemmati, M. Lafouti, *Opt. Lasers Eng.* **2012**, *50*, 293.
[17] W. Song, Y. Xie, W. Hao, J. Han, P. Yan, X. Li, Y. Wang, X. Li, C. Sun, Z. Li, *Opt. Laser Technol.* **2023**, *162*, 109245.
[18] Y. G. Lee, C. H. Park, S. W. Back, H. J. Kim, S. S. Lee, *Appl. Opt.* **2016**, *55*, 341.
[19] N. Yu, P. Genevet, M. A. Kats, F. Aieta, J. P. Tetienne, F. Capasso, Z. Gaburro, *Science* **2011**, *334*, 333.
[20] N. Li, Y. Fu, Y. Dong, T. Hu, Z. Xu, Q. Zhong, D. Li, K. Lai, S. Zhu, Q. Lin, Y. Gu, N. Singh, *Nanophotonics* **2019**, *8*, 1855.
[21] Y. Chen, J. Gao, X. Yang, *Laser Photonics Rev.* **2018**, *12*, 1800198.
[22] S. Q. Li, X. Xu, R. Maruthiyodan Veetil, V. Valuckas, R. Paniagua-Domínguez, A. I. Kuznetsov, *Science* **2019**, *364*, 1087.
[23] W. T. Chen, K. Y. Yang, C. M. Wang, Y. W. Huang, G. Sun, I. D. Chiang, C. Y. Liao, W. L. Hsu, H. T. Lin, S. Sun, L. Zhou, A. Q. Liu, D. P. Tsai, *Nano Lett.* **2014**, *14*, 225.
[24] J. Y. Yang, I. Ghimire, P. C. Wu, S. Gurung, C. Arndt, D. P. Tsai, H. W. H. Lee, *Nanophotonics* **2019**, *8*, 443.
[25] M. Principe, M. Consales, A. Micco, A. Crescitelli, G. Castaldi, E. Esposito, V. L. Ferrara, A. Cutolo, V. Galdi, A. Cusano, *Light: Sci. Appl.* **2017**, *6*, e16226.
[26] Z. Ding, H. Xu, Y. Xiong, K. Zhou, Y. Chen, Y. Lu, F. Xu, *Adv. Opt. Mater.* **2022**, *10*, 2201724.
[27] P. Vaiano, B. Carotenuto, M. Pisco, A. Ricciardi, G. Quero, M. Consales, A. Crescitelli, E. Esposito, A. Cusano, *Laser Photonics Rev.* **2016**, *10*, 922.
[28] M. Scaravilli, A. Micco, G. Castaldi, G. Coppola, M. Gioffre, M. Iodice, V. L. Ferrara, V. Galdi, A. Cusano, *Adv. Opt. Mater.* **2018**, *6*, 1800477.
[29] D. G. Kotsifaki, S. N. Chormaic, *Nanophotonics* **2019**, *8*, 1227.
[30] M. Juhl, J. P. B. Mueller, K. Leosson, *IEEE J. Sel. Top. Quantum Electron.* **2019**, *25*, 4500107.
[31] P. C. Wu, W. M. Zhu, Z. X. Shen, P. H. J. Chong, W. Ser, D. P. Tsai, A. Q. Liu, *Adv. Opt. Mater.* **2017**, *5*, 1600938.
[32] C. Zhou, W. B. Lee, S. Gao, H. Li, C. S. Park, D. Y. Choi, S. S. Lee, *Laser Photonics Rev.* **2021**, *15*, 2000581.
[33] H. Li, S. Gao, Y. Li, C. Zhang, W. Yue, *Opt. Express* **2019**, *27*, 35027.
[34] Z. Jiang, J. R. Marciante, *J. Lightwave Technol.* **2006**, *24*, 1350.
[35] H. Ye, Q. Sun, Z. Guo, Y. Hou, F. Wen, D. Yuan, F. Qin, G. Zhou, *Opt. Express* **2021**, *29*, 27521.
[36] Y. Y. Xie, P. N. Ni, Q. H. Wang, Q. Kan, G. Briere, P. P. Chen, Z. Z. Zhao, A. Delga, H. R. Ren, H. D. Chen, C. Xu, P. Genevet, *Nat. Nanotechnol.* **2020**, *15*, 125.
[37] J. Alda, *Encyclopedia Opt. Eng.* **2003**, *999*, 1013.

[38] R. A. Lymarenko, D. Gailevicius, I. Meskelaite, L. Grineviciute, M. Peckus, K. Staliunas, V. B. Taranenko, *Opt. Lett.* **2021**, *46*, 3845.
[39] L. Meng, L. Yuan, *Opt. Laser Technol.* **2024**, *174*, 110582.
[40] X. Chen, K. Li, Q. Wu, J. Clark, J. E. Hurley, J. S. Stone, M. J. Li, *Opt. Fiber Technol.* **2022**, *69*, 102848.
[41] O. A. Jimenez Gordillo, S. Chaitanya, Y. C. Chang, U. D. Dave, A. Mohanty, M. Lipson, *Opt. Express* **2019**, *27*, 20305.
[42] L. Monroy, M. Soriano-Amat, Ó. Esteban, E. Monroy, M. González-Herráez, F. B. Naranjo, *Opt. Express* **2021**, *29*, 29357.
[43] Q. He, Z. Zhao, X. Ye, C. Luo, D. Zhang, S. Wang, X. Xu, *Micromachines* **2022**, *13*, 324.
[44] X. Dong, P. Li, X. Zhang, W. Yang, *Laser Optoelectron. Prog.* **2020**, *57*, 152201.
[45] G. Keiser, *Optical Fiber Communications*, 3rd ed., McGraw-Hill, New York **2000**.